Kinetic Modeling of Jet Propellant-10 Pyrolysis

Nick M. Vandewiele,[†] Gregory R. Magoon,[‡] Kevin M. Van Geem,[†] Marie-Françoise Reyniers,*,[†] William H. Green,[‡] and Guy B. Marin[†]

[†]Laboratory for Chemical Technology, Universiteit Gent, Technologiepark 914, B-9052 Gent, Belgium
[‡]Department of Chemical Engineering, Massachusetts Institute of Technology, Cambridge, Massachusetts 02139, United States

Ⓢ *Supporting Information*

ABSTRACT: A detailed kinetic model for the thermal decomposition of the advanced fuel Jet-Propellant 10 (JP-10) was constructed using a combination of automated mechanism generation techniques and *ab initio* calculations. Rate coefficients for important unimolecular initiation routes of *exo*-TCD were calculated using the multireference method CAS-PT2, while rate coefficients for the various primary decompositions of the *exo*-TCD-derived monoradicals were obtained using CBS-QB3. Rate-of-production analysis showed the importance of four dominating JP-10 decomposition channels. The model predictions agree well with five independent experimental data sets for JP-10 pyrolysis that cover a wide range of operating conditions ($T = 300-1500$ K, $P = 300$ Pa-1.7×10^5 Pa, dilution = 0.7$-$100 mol% JP-10, conversion = 0$-$100%) without any adjustment of the model parameters. A significant part of the model comprises secondary conversion routes to aromatic and polyaromatic hydrocarbons and could thus be used to assess the tendency for deposit formation in fuel-rich zones of endothermic fuel applications.

1. INTRODUCTION

Mono- and polycyclic hydrocarbons represent an interesting class of molecules that can be used as fuels in advanced aviation applications.[1] Many of them have superior physical properties such as a high energy content, a low viscosity at low temperatures, an elevated flash point, and a higher density compared to the classically used *n*-alkanes.[2,3] Cyclic alkanes also have higher thermal stability limits and a larger heat sink capacity than their acyclic counterparts (cf. *n*-decane vs decalin in ref 4), which are important properties in the propulsion technology. Endothermic cracking of the fuel prior to the combustion chamber[5−7] not only amplifies the heat sink but can also reduce ignition delays, as illustrated by Colket et al.[8] Hence, a thorough understanding of the decomposition chemistry of cyclic hydrocarbons is important not only for the design and optimization of the endothermic reaction technology itself, but also for the correct design of the combustor that converts the products of the endothermic decomposition.

This study focuses on the kinetic modeling of the thermal decomposition of the fuel Jet Propellant-10 (JP-10), used as the fuel for air-breathing missiles.[9] JP-10 consists of a tricyclic hydrocarbon, *exo*-tricyclo[5.2.1.0^{2,6}]decane (*exo*-TCD), cf. Scheme 1.

Although a fair number of experimental JP-10 pyrolysis studies identified and quantified light products containing up to

five carbons,[10−15] less is known about the quantities of heavier intermediates and products. Several studies noted the significant formation of aromatic components such as benzene and toluene under pyrolysis conditions.[10,12−16] Even in the presence of an oxidizer, aromatic components represented an important share of the products, as the comparative study between the flame structure of *n*-decane and JP-10 flames[17] indicated. Vandewiele et al.[18] obtained a new data set of JP-10 pyrolysis experiments using GC×GC-FID/ToF-MS, in which over 70 species with mass-to-charge ratio up to 178 (C$_{14}$H$_{10}$) were identified and quantified. Validation of two available kinetic models of JP-10 thermal decomposition, the San Diego model[19] and the model by Magoon et al.,[20] revealed that they were largely inadequate in accurately predicting product distribution trends of the experiments of Vandewiele et al.[18] This is not surprising since these kinetic models were designed for higher temperature combustion applications and not for the pyrolysis conditions investigated in that study. Herbinet et al. reported a pyrolysis model for JP-10, but that model is not publicly available.[10]

It is thus clear that an accurate kinetic model for the purpose of modeling JP-10 pyrolysis is currently not available in the open literature. Therefore, a new dedicated pyrolysis model was constructed with the help of the Reaction Mechanism Generator (RMG).[21] To further elucidate the initial decomposition of *exo*-TCD, a large number of electronic structure calculations were carried out for reactions for which accurate reaction rate coefficients are missing. Five experimental data sets that encompass a wide range of operating conditions were used for the validation of the model.

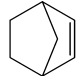**Scheme 1.** *exo*-Tricyclo[5.2.1.0^{2,6}]decane (*exo*-TCD), the Main Constituent of JP-10
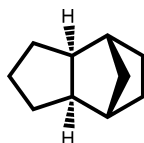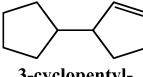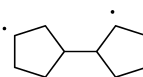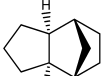
Table 1. Comparison of the Thermochemical Properties for Selected Polycyclic Species from the Following Methods: (1) PM3 Method Implemented through RMG with On-the-Fly Generation of Atomic Coordinates (RMG-PM3); (2) Benson Group Additivity Method Implemented in RMG Including Polycyclic Ring Strain Corrections (RMG-GA); and (3) Benchmark Values from Either *ab Initio* Calculations or Experimental Data

Component		$\Delta_f H°$ (298K)	$S°$ (298K)	$C_p°$ (298K)	$C_p°$ (800K)	$C_p°$ (1500K)
		kJ mol^{-1}	J K^{-1}mol^{-1}			
2-Norbornene	Benchmark	80[48]	306[#]	112.7[49]	268.2[49]	344[#]
	RMG-PM3	92	306	100	260	343
	RMG-GA	80	188	121	272	352
Norbornane	Benchmark	-54.9±1.1[50]	313[#]	120[49]	296[49]	382[#]
	RMG-PM3	-59	306	105	289	381
	RMG-GA	-50	193	134	301	389
3-cyclopentyl-cyclopentene (MA110)	THERGAS	-4	431	167	406	536
	RMG-PM3	-54	422	163	406	532
	RMG-GA	-13	423	163	402	527
BR1	UB3LYP/cbsb7 [10]	243	410	180	410	536
	RMG-PM3	218	467	159	398	527
	RMG-GA	251	481	155	389	523
tricyclodecyl radical (TCDR8)	CBS-QB3[47]	113	364	155	389	511
	RMG-PM3	105	377	142	385	511
	RMG-GA	134	377	142	385	511

[#]Based on B3LYP calculation, this study.

2. COMPUTATIONAL METHODS

2.1. Kinetic Model Construction. Fully automated kinetic model generation is not possible at present. Significant user involvement is still required to obtain an accurate model. Fortunately, automatic network generation programs can reduce part of the burden if the relevant reaction families are known and thermochemical and kinetic data are available. Reaction Mechanism Generator (RMG)[22,23] is an open-source software package that automatically constructs kinetic models on the basis of the evaluation of reaction rates and species concentrations. The procedure used by RMG to expand the kinetic model by successive addition of kinetically significant species[24] is extensively discussed elsewhere (e.g., refs 25−27), and therefore only the elements specific to the modeling of the pyrolysis of polycyclic hydrocarbons are highlighted here. Temperature, pressure, and initial *exo*-TCD dilution, which are used to evaluate rates of production in RMG, are set to 1100 K, 1 × 10⁵ Pa, and 10 mol%, respectively. The main parameters determining the size of the generated reaction network, i.e., the time at which the integration of the ODEs is stopped and tolerance ε for the network generation, were set to 0.5 s and 0.001, respectively. For these conditions the most important products observed in the experiments are included in the reaction network. The use of tighter tolerances significantly increases the size of the model but does not affect the model predictions. The effect of both parameters on the size of the reaction network for steam-cracking of *n*-hexane was illustrated by Van Geem et al.[27]

RMG was previously employed to construct a model for combustion applications of JP-10.[20] The model described in this work is not an update of that combustion model but was built from scratch for endothermic fuel applications of JP-10 and aims at elucidating a complementary part of the thermal decomposition chemistry of JP-10. The pyrolysis of *exo*-TCD is described mainly by three elementary reaction families: intermolecular hydrogen abstraction reactions by radicals, intra- and intermolecular radical addition reactions, and intermolecular radical recombination reactions. Details of the rate rules of these reaction families can be found elsewhere.[22,23] Note that the reactions belonging to the reverse reaction families, i.e., β-scission reactions and unimolecular scission reactions, are allowed, too; rate coefficients of these reactions are calculated on the basis of thermodynamic consistency.

In addition to built-in databases for reaction families, a number of reactions from the literature were added that contain relevant *exo*-TCD pyrolysis chemistry. First, two submodels were added that contain chemistry of species with two carbon atoms or less using the seed mechanism option in RMG. The Leeds methane oxidation model v1.5,[28] stripped of all oxygen chemistry, was used as a base model for high-temperature pyrolysis reactions, resulting in 34 reactions between 22 species. An ethane steam-cracking model by Sabbe et al.,[26] stripped of all reactions containing four or more carbons, was used as a base model for the low-temperature pyrolysis and contains 277 reactions between 35 species. Next, a number of literature submodels were added to RMG through the so-called "Reaction Library" option of RMG. The reactions in these submodels are considered during the iterative enlargement procedure and are added to the final model based on the kinetic significance of the species of these reactions. These literature submodels can be divided into two categories. First, sources of cyclic C_5−C_6−C_7 chemistry[29,30] were included, as it is believed that they are crucial in bridging the gap between the *exo*-TCD decomposition products and secondary products such as aromatics. Second, sources were included that contain pathways for the growth of polycyclic aromatic hydrocarbons (PAHs) such as indene and naphthalene.[31,32] Finally, 33 *exo*-TCD decomposition reactions were added, primarily originating from new transition-state theory (TST) calculations performed in this study. In cases where two seed mechanisms included rate coefficients for the same reaction, the choice of the retained rate coefficients is determined on a case-per-case basis based on the date of publication, the associated uncertainty of the level-of-theory for rate coefficients obtained through computational

Table 2. Summary of Operating Conditions of the Experimental Data Sets Used for Model Validation

	Nakra data[13]	Van Devener data[14]	Nancy data[10]	Rao data[12]	Xing data[15]	Ghent data[18]
pressure/Pa	300−400	1500−1900	1×10^5	1×10^5	$1−37 \times 10^5$	1.7×10^5
residence time[b]/ms	2−10	3−10	500−6000	700−6400	480−26400	300−500
mol% exo-TCD, in inert gas	2.6, Ar	3.9, Ar	0.7−4, He	100[a]	100[a]	7/10, N_2
temperature range/K	300−1500	300−1400	848−933	903−968	823−903	930−1080
conversion range/%	0−100	0−100	0.01−25	10−60	0−25	4−94
reactor type	plug flow	plug flow	CSTR	plug flow	plug flow	plug flow
endo-TCD content/%	N/R[d]	N/R[d]	2.5	3.6[c]	0.23	0.6

[a]No diluent present. [b]Residence time based on the total (including diluent) molar flow rate at the entrance of the reactor, at the mean temperature inside the reactor. [c]Based on reported 96.4% purity of reactant. [d]Not reported.

chemistry techniques, and the degree of experimental validation that was provided. More information on the kinetic model development is provided in Section S1 of the Supporting Information.

The automated calculation of pressure-dependent rate coefficients of reactions by RMG was not applied for this study. As a result, the assigned rate coefficients of the generated reactions in the model should be treated as high-pressure limits. Nevertheless, 20 reactions originating from ad hoc added reaction libraries have pressure-dependent rate expressions.

2.2. Thermochemistry. A detailed decomposition model necessitates the inclusion of thermochemical parameters for all intermediate species. This can be achieved on the basis of group and bond additivity methods,[33] but the accuracy of these estimates may be doubtful for species with structures that fall beyond the scope of the regressed group additive parameters. More specifically, the influence of ring strain on the thermochemistry estimates of polycyclic intermediates remains a point of concern. Magoon et al.[34,35] addressed this issue by incorporating on-the-fly thermochemical calculations for polycyclic intermediates using three-dimensional atomic coordinates in molecules.[20] In the present work, several important modifications in the calculation of thermochemical parameters for polycyclic intermediates were incorporated. First, a database of polycyclic ring strain corrections (RSC) was added containing ca. 100 polycyclic structures.[36−40] If an appropriate polycyclic RSC is found for a component, it is used in the estimation of the thermochemical parameters. If not, the molecule is passed on to the framework that generates 3D atomic coordinates on-the-fly using a distance−geometry algorithm implemented in the chemoinformatics toolkit RDKit[41] to convert the chemical graph representation into a 3D geometry. Second, the database of hydrogen bond increments (HBIs), a method developed by Lay et al.[42] to estimate the thermochemistry of radicals, was expanded with groups for cyclic and polycyclic radicals found in literature.[43−46] The radical atom in strained species cannot adopt the energetically favored planar geometry because of the constriction of the rigid carbon frame and therefore significantly alters the value of the corresponding HBI in comparison with the acyclic analogue. Table 1 shows a comparison of the thermochemistry estimates for a selected set of polycyclic strained species relevant for exo-TCD decomposition. Three values are reported: the Benson group additivity method including polycyclic ring strain corrections (RMG-GA), the semi-empirical PM3 method using 3D atomic coordinates that are generated on-the-fly (RMG-PM3), and finally the best available benchmark value. It was observed that neither RMG-GA nor RMG-PM3 reproduces all benchmark data well. In general, RMG-GA scores better for enthalpies of formation than for entropies or heat capacities because more data are available in literature. In the worst case, S and C_p contributions of polycyclic RSCs were estimated as a sum of contributions of smaller rings. The example of norbornene illustrates this principle. The value of the standard enthalpy of formation at 298 K, estimated through RMG-GA, corresponds well with the benchmark value, whereas significant differences are observed for the standard entropy at 298 K. The values for the enthalpy contribution to the norbornene RSC originate from Wiberg.[37] Due to the lack of values for the entropy contribution of the norbornene RSC, the value is taken as equal to the cyclopentane RSC. Note that the thermochemistry of species in the model is always based on the best available estimates,

e.g., CBS-QB3 values for the six tricyclodecyl $C_{10}H_{15}$ radicals from ref 47.

2.3. Ab Initio Calculations. High-level thermochemical data for species involved in the JP-10 thermal decomposition are very scarce. Rate coefficients are even less available, in particular regarding the initial decomposition of exo-TCD. Therefore, in this work new high-level ab initio calculations were carried out on a set of reactions that are believed to be important for the decomposition of exo-TCD. Three types of reactions were considered.

Unimolecular C−C scission reactions of exo-TCD leading to biradicals and subsequent intramolecular H-abstraction reactions of the biradicals were explored using density functional theory (DFT) and multireference methods. In the DFT methodology, geometries were optimized using UB3LYP (unrestricted B3LYP), and energies were calculated using CBS-QB3 to explore the PES and obtain initial refinements of kinetic parameters. Using the DFT geometries as initial guesses, a multireference methodology, CASPT2,[51,52] a second-order perturbation theory, multireference counterpart of the MP2 method, as implemented in MOLPRO,[53] was applied. A four-electron, four-orbital active space, generally corresponding to the electrons and orbitals of interest for these reactive transformations, as described in ref 20, was employed. In contrast to the previous study,[20] which relied on CASSCF reaction path geometries for performing higher-level single-point calculations, the saddle points and minima considered here were obtained directly on the higher level, in this case CASPT2. A 6-311G(d,p) basis set, as used by Sirjean et al. in CASSCF studies of similar reactions,[54,55] was applied here. Hessian/frequency calculations at the minima and saddle points were performed using finite differencing of analytic CASPT2 gradients, as calculated by MOLPRO. Partition functions were computed with the rigid-rotor, harmonic oscillator (RRHO) approximation, and Arrhenius parameters were obtained using conventional TST.

A third type of reaction is the unimolecular C−C and C−H β-scission of tricyclodecyl ($C_{10}H_{15}$) monoradicals. These reactions were studied on the CBS-QB3 level of theory using Gaussian03 and Gaussian09. Tricyclodecyl reactant structures were optimized with "verytight" convergence criteria; correspondingly, a very fine integration grid was used ("int=ultrafine"). Vibrational frequencies, calculated at the B3LYP/CBSB7 level of theory, confirmed that the transition state (TS) structures were saddle points of first order and have a single imaginary frequency. Geometries were visually inspected to confirm that the structure was intermediate between the intended reactant and product(s). Conventional TST calculations were performed using results for the saddle point and corresponding tricyclodecyl reactant. A table with reaction barriers at 0 K for the reactions calculated in this work is available in Section S2 of the Supporting Information. Quantum tunneling coefficients were calculated by employing the symmetric Eckart tunneling scheme with energetic information from tricyclodecyl reactant and the saddle point.[56] Frequencies were corrected by a scaling factor of 0.99. These TST calculations were performed using the software package CanTherm.[57] Rate coefficients were computed at 10 different temperatures ranging from 298 to 3000 K. Based on these sampled points, a three-parameter least-squares fit was performed to determine the parameters for a modified Arrhenius rate coefficient expression. A discussion of the uncertainties associated with the three-parameter fit

of the modified Arrhenius parameters is given in Section S3 of the Supporting Information.

3. REACTOR MODELING AND EXPERIMENTAL DATA

A wide variety of experimental data on the thermal decomposition of *exo*-TCD published in open literature were used for validating the model. The kinetic model was compared to the product distribution data obtained by Herbinet et al.[10] (hereafter referred to as the "Nancy data"), Nakra et al.[13] ("Nakra data"), Van Devener and Anderson[14] ("Van Devener data"), Rao and Kunzru ("Rao data"),[12] Xing et al.[15] ("Xing data"), and Vandewiele et al.,[18] referred to as "Ghent data" in this work. Table 2 shows an overview of the operating conditions of each experimental data set.

Reactor simulations were systematically conducted with the Chemkin Pro package.[58] The experiments of Herbinet et al.[10] performed in a jet-stirred reactor were modeled with a perfectly mixed reactor model, similar to what was done in their comparison with the Nancy model. The steady-state reactor model was solved using a reactor volume of 90 cm^3 and a given temperature and pressure. The data from Nakra et al.[13] and Van Devener and Anderson[14] were collected at millisecond time scale under reduced pressure. Both reactors were modeled as plug flow reactors specifying the given diameter and length of the hot zone in the reactor. Isothermal and isobaric conditions with the pressure based on the provided hot zone midpoint pressure were used. In the continuous flow tubular reactor of Rao and Kunzru[12] the axial temperature profile along the reactor was not reported. Instead, the equivalent reactor temperature, i.e., the temperature at which the same *exo*-TCD conversion would be attained as in the non-isothermal case, was provided. Therefore, the reactor was modeled using isothermal, isobaric boundary conditions. Xing et al.[15] reported JP-10 pyrolysis data up to pressures of 37 × 10^5 Pa. Because species fractions were reported for the gaseous and liquid phase separately, without any indication of the relative ratio of the two phases, only *exo*-TCD conversion was compared. The flow reactor was modeled as a plug flow reactor using isothermal, isobaric boundary conditions. Vandewiele et al. reported experiments in a continuous flow tubular reactor.[18] Radial temperature and concentration gradients were shown to be negligible using two-dimensional reactor models for this reactor,[25,59] so it was also modeled as an ideal plug flow reactor. For all the flow reactor experiments modeled in this work, the integration was stopped at the reported space time.

JP-10 feedstock contains a number of impurities, such as *endo*-tricyclo[5.2.1.0^{2,6}]decane (*endo*-TCD), adamantane and decalin in decreasing order of importance. While the cumulative content of these impurities typically does not exceed 3.5% of JP-10 feedstock,[60] the presence of *endo*-TCD may be of importance for the reactivity of *exo*-TCD. Hudzik et al.[47] reported that the standard enthalpy of formation of *endo*-TCD is 17 kJ mol^{-1} higher than the value for *exo*-TCD, suggesting that the *endo*-isomer may be less stable than the *exo*-isomer. Information on the initial decomposition of *endo*-TCD is nonexistent in the literature; therefore, only one reaction was added that converts *endo*-TCD into BR1, similar to the initiation of *exo*-TCD.

The activation energy of this reaction is lowered by 17 kJ mol^{-1}, relative to the value of the reaction with *exo*-TCD, to reflect the higher enthalpy of formation of the *endo*-isomer. The JP-10 feedstock of the modeled experiments was treated as a mixture of exo- and *endo*-TCD whenever information on the


endo-TCD **BR1**
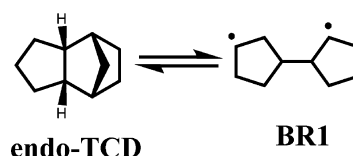
content of *endo*-TCD was available, cf. Table 2. If not, JP-10 was considered as 100% *exo*-isomer.

## 4. RESULTS AND DISCUSSION

The final RMG-generated, kinetic model for the pyrolysis of *exo*-TCD contains 5261 reactions between 384 species, i.e., 234

Scheme 2. *exo*-TCD Initiation Routes through Unimolecular C−C Scission Reactions Resulting in Seven Biradicals, BRx, x = 1, ..., 7^a
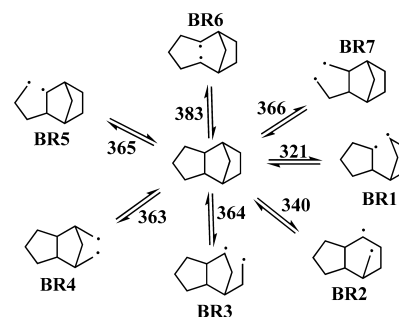
^{a}Nomenclature for the biradicals is adopted from Herbinet et al.[10] Values represent standard reaction enthalpies (kJ mol^{-1}) at 298 K, based on thermochemistry used in this model.

Scheme 3. Unimolecular C−C Scission of *exo*-TCD Yielding Biradicals and Subsequent Intramolecular H-Abstraction Reactions Yielding Molecular Intermediates Taken into Account in This Work
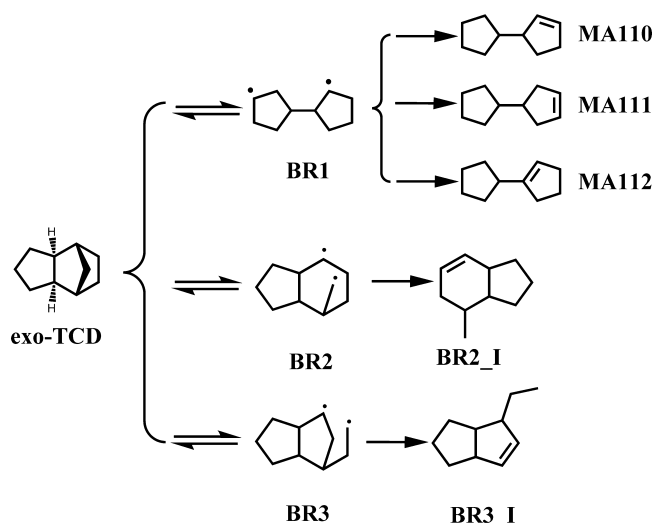

radicals and 150 molecular species, and can be found in Section S4 of the Supporting Information. Thermochemistry of 18% of the cyclic species in the model was estimated via PM3 calculations, 19% from literature while the remainder was estimated via group contribution methods. The model consists of 4308 H-abstraction reactions, 316 radical addition reactions to molecules with double or triple bonds, 158 radical recombination reactions, the remaining 479 reactions origi-

Table 3. Rate Coefficients for *exo*-TCD Initiation Reactions and Intramolecular H-Abstraction Reactions[a]

reaction	A	n	E_a	method used
		exo-TCD Initiation Reactions		
exo-TCD = BR1	1.80×10^{13}	0.83	326	CAS-PT2[c]
exo-TCD = BR1	7.09×10^{12}	0.97	319	UB3LYP/CBS-QB3
exo-TCD = BR1	5×10^{15}	0	322	Herbinet et al.[10]
exo-TCD = BR2c[b]	8.32×10^{10}	1.87	333	CAS-PT2[c]
exo-TCD = BR2d[b]	1.09×10^{13}	0.80	325	CAS-PT2[c]
exo-TCD = BR2c[b]	5.06×10^{12}	0.96	328	UB3LYP/CBS-QB3
exo-TCD = BR2d[b]	3.87×10^{12}	0.95	321	UB3LYP/CBS-QB3
exo-TCD = BR2	5×10^{15}	0	297	Herbinet et al.[10]
exo-TCD = BR3	6.09×10^{12}	0.92	335	CAS-PT2[c]
exo-TCD = BR3	3.40×10^{12}	1.09	334	UB3LYP/CBS-QB3
exo-TCD = BR3	5×10^{15}	0	322	Herbinet et al.[10]
exo-TCD = BR4	8.05×10^{12}	1.24	334	UB3LYP/CBS-QB3[c]
exo-TCD = BR4	5×10^{15}	0	322	Herbinet et al.[10]
exo-TCD = MA110	5.76×10^{10}	6.88	416	UB3LYP/CBS-QB3[c]
exo-TCD = MA111	1.85×10^{11}	1.23	336	UB3LYP/CBS-QB3[c]
		Intramolecular H-Abstraction Reactions		
BR1 = MA110	8.64×10^{11}	0.08	−1	CAS-PT2[c]
BR1 = MA110	2.90×10^{10}	0.44	15	UB3LYP/CBS-QB3
BR1 = MA110	1.9×10^{10}	1	32	Herbinet et al.[10]
BR2 = BR2_I	4.5×10^{9}	0.65	20	UB3LYP/CBS-QB3[c]
BR3 = BR3_I	2.87×10^{10}	0.40	23	UB3LYP/CBS-QB3[c]

[a]Rate coefficient k is expressed as $k = AT^n \exp(-E_a/RT)$. Arrhenius parameters are fitted for a temperature range from 298 to 3000 K. Unit for A is s^{-1}, and unit for E_a is kJ mol^{-1}. [b]For BR2, two reactions are identified corresponding to two different BR2 product conformers. [c]denotes the rate coefficient used in the current model.

Scheme 4. Six Possible $C_{10}H_{15}$ Tricyclodecyl Radicals Created by H-Abstraction Reactions from *exo*-TCD[a]
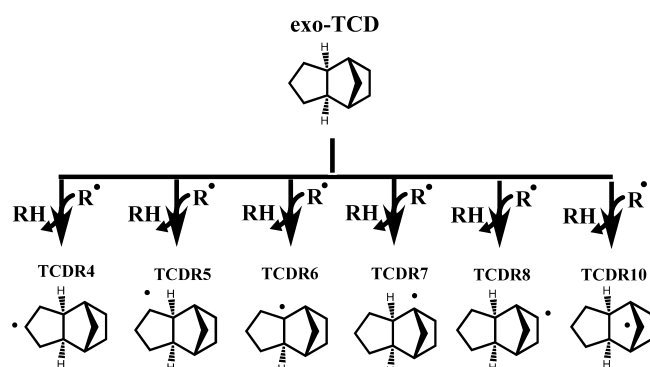
[a]Nomenclature for the tricyclodecyl monoradicals is adopted from Hudzik et al.[47]

nated from specific libraries, as was previously discussed, including 7 ring-opening reactions, 3 intramolecular H-abstraction reactions, and 33 β-scission reactions calculated in this work.

4.1. Primary Decomposition Chemistry. *4.1.1. exo-TCD Initiation.* It is generally assumed that the pyrolysis of hydrocarbons such as *exo*-TCD proceeds through a free radical mechanism. The initiation of *exo*-TCD involves the creation of radicals through unimolecular bond scission reactions of *exo*-TCD. Although the rupture of C−H bonds is possible as an *exo*-TCD initiation route, these bonds are stronger than C−C bonds and were consequently neglected. The unimolecular initiation of *exo*-TCD can proceed through unimolecular C−C bond scission reactions resulting in the creation of seven distinct biradicals named BRx, x = 1, ..., 7, cf. Scheme 2.

The resulting highly unstable biradicals can further isomerize to stable molecules via intramolecular H-abstraction reactions (disproportionation reactions), proposed by Herbinet et al.[10] upon detecting 3-cyclopentylcyclopentene, further referred to as "MA110", as a major primary decomposition product.

Intramolecular H-abstraction reactions are thought to proceed via multiple distinct TSs that differ by the polycyclic entity that is formed through the course of the reaction, cf. Scheme 3.

Herbinet et al.[10] were among the first to estimate both the ring-opening reactions and the intramolecular H-abstraction reactions via semiempirical correlations based on observations by O'Neal and Benson,[61] in which the ring strain of reactants, products, and TSs played a central role. These qualitative estimations were combined with thermochemistry estimated via Benson group additivity and showed that the initiation route via BR1 to MA110 was significantly faster than the other competing initiation routes. More recently, Magoon et al.[20] discussed the difficulty in accurately quantifying reaction barriers for the intramolecular disproportionation reactions. *Ab initio* calculations performed by Magoon et al.[20] suggested there may be a very small barrier or even no barrier at all. So, Magoon et al.[20] suggested that initiation of *exo*-TCD toward MA110 may proceed as a concerted step rather than via a distinct biradical intermediate.[20] In the present work, rate coefficients for 10 ring-opening and intramolecular H-abstraction reactions were calculated. The latter are particularly useful in the re-evaluation of the relative importance of the different *exo*-TCD initiation routes. Table 3 shows values for the Arrhenius parameters for these reactions.

Activation energies for the ring-opening reactions are similar to those reported by Herbinet et al.[10] The good agreement between the *ab initio* and semiempirical values also shows that the estimation of activation barriers based on the difference in
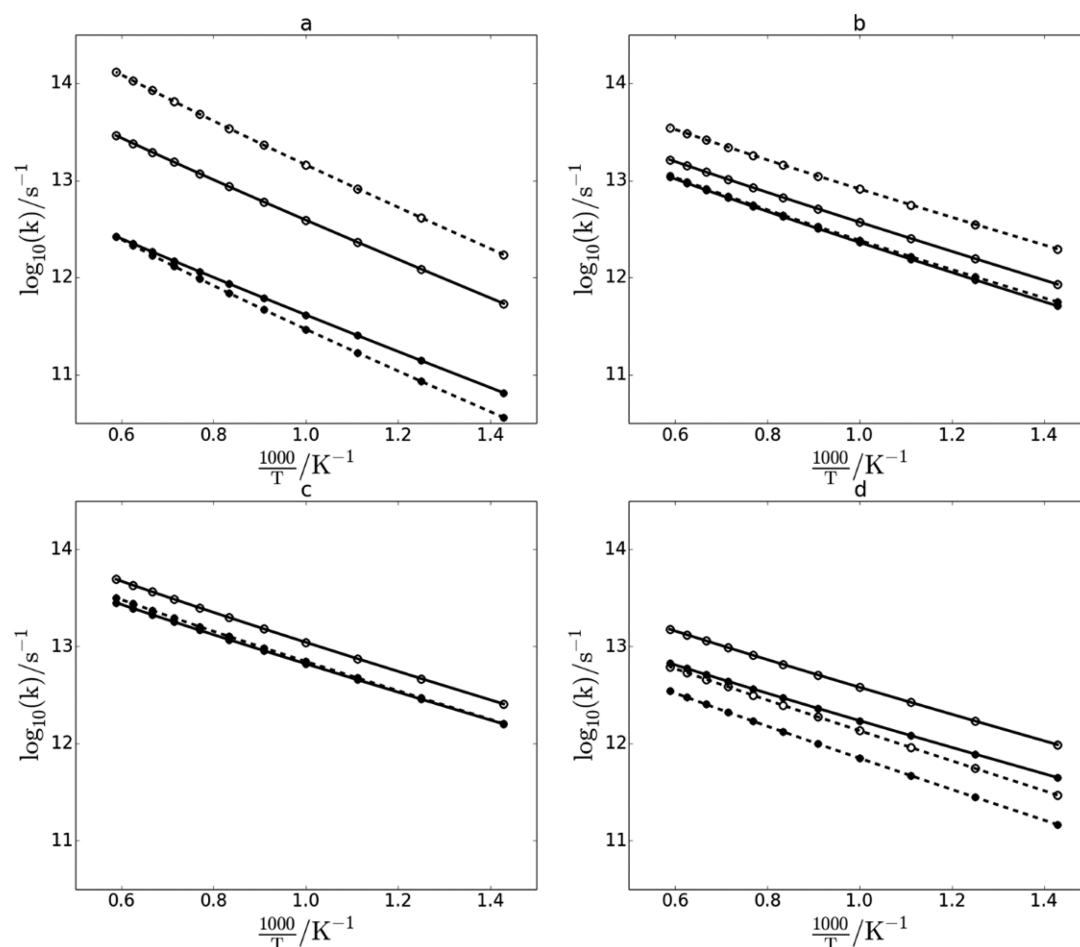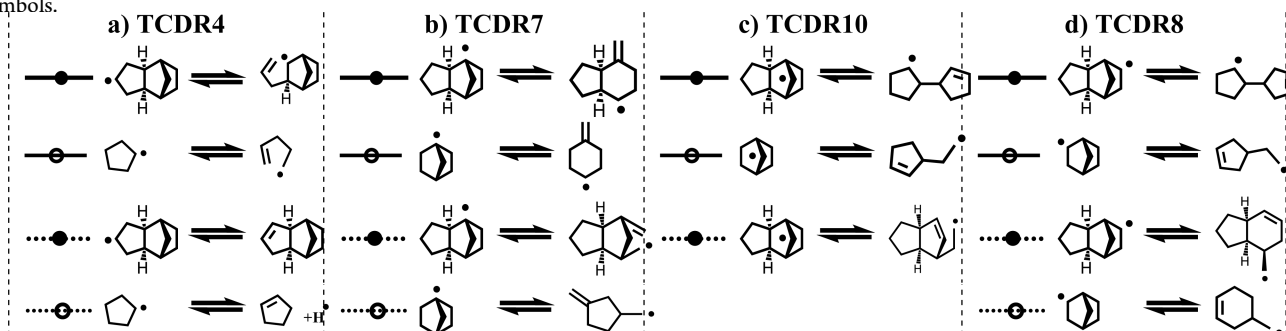
Figure 1. Rate coefficients as a function of temperature. Cyclopentyl and norbornyl decomposition reaction rate coefficients from Sirjean et al.[63,64] Tricyclodecyl decomposition reaction rate coefficients calculated in this work. Tricyclodecyl decomposition reactions are represented by full symbols.

ring strain between the reactant and product is acceptable as a first approximation. Values for the initiation of *exo*-TCD leading to the formation of BR2 are the exception where the current calculations indicate an activation barrier that is comparable to the other scission possibilities while the Herbinet et al. estimates[10] are ca. 30 kJ mol⁻¹ lower. Good agreement for the ring-opening reactions between the CBS-QB3 values and the CAS-PT2 values for activation energies show the usefulness of the less expensive CBS-QB3 method for these kinds of calculations. Re-evaluation of the global decomposition rates of *exo*-TCD via the initiation and corresponding subsequent disproportionation channels confirms that the initiation route via BR1 to MA110 is 2 orders of magnitude faster than the competing channels via BR2 and

BR3, implying that this channel is the principal unimolecular initiation route for *exo*-TCD at temperatures around 1000 K. This is in line with conclusions by Herbinet et al.[10] The concerted pathway from *exo*-TCD to MA110, using the kinetics by Magoon et al.[20] is significantly slower than the route via biradical BR1. Finally, despite the lesser stability of *endo*-TCD, and the faster ring-opening kinetics of *endo*-TCD relative to *exo*-TCD, the presence of *endo*-TCD in the JP-10 feedstock did not have a significant influence on the initiation of *exo*-TCD at the experimental conditions studied in this work.

4.1.2. Tricyclodecyl Decomposition Reactions. It is expected that a large part of *exo*-TCD conversion is attributed to H-abstraction reactions by radicals. The abstraction of a hydrogen atom from *exo*-TCD yields six distinct $C_{10}H_{15}$
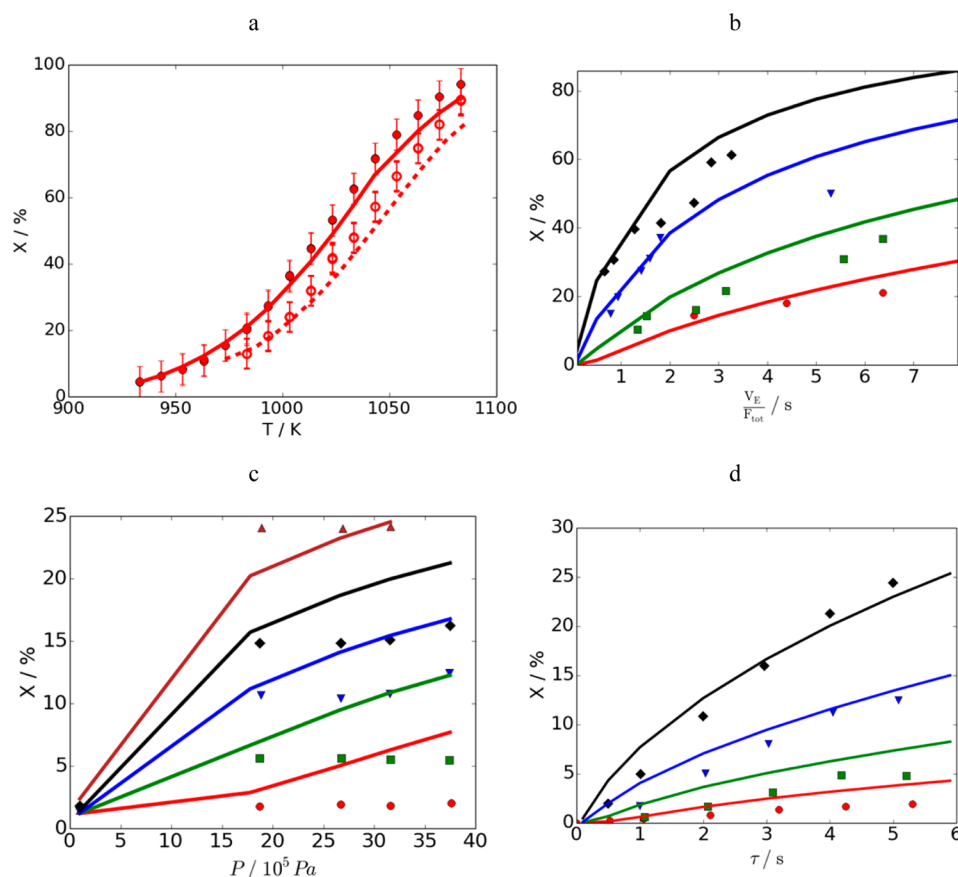
Figure 2. (a) JP-10 conversion as a function of temperature for two dilution levels of JP-10 in N_2 at the reactor inlet for the Ghent data:[18] (● and —) 10 mol% and (○ and ---) 7 mol% JP-10 in N_2; $P = 1.7 \times 10^5$ Pa. (b) JP-10 conversion as a function of equivalent space time for the Rao data[12] at different temperatures: ◆, 968; ▼, 948; ■, 923; and ●, 903 K. Conditions: 100% JP-10 at the reactor inlet, $P = 1 \times 10^5$ Pa, $T = 903-968$ K. (c) JP-10 conversion as a function of reactor pressure for the Xing data[15] at different temperatures: ▲, 903; ◆, 883; ▼, 863; ■, 843; and ●, 823 K. Conditions: 100% JP-10 at the reactor inlet, $T = 823-903$ K. (d) JP-10 conversion as a function of residence time for the Nancy data[10] at different temperatures: ◆, 933; ▼, 913; ■, 893; and ●, 873 K. Conditions: 4 mol% *exo*-TCD in He at the reactor inlet, $T = 848-933$ K, $P = 1 \times 10^5$ Pa, conversion = 0.01−25%. Symbols are experimental data, and lines are model predictions.

tricyclodecyl radicals, cf. Scheme 4. The kinetics of these H-abstractions not only greatly affect the *exo*-TCD conversion, but they also determine selectivity of the primary products since each tricyclodecyl radical leads to distinct primary products. The activation energy of the H-abstraction reactions by H atoms from *exo*-TCD were calculated using an Evans−Polanyi relationship proposed by Dean and Bozzelli.[62] The instability induced by the strained nature of the resulting tricyclodecyl radicals was thus taken into account in the kinetics of these hydrogen abstraction reactions.

The tricyclodecyl radicals subsequently react via various C−H and C−C β-scission reactions leading to either $C_{10}H_{14}$ molecules or new $C_{10}H_{15}$ radicals. A single monoradical can react through multiple parallel decomposition channels. The kinetics for these elementary reactions were not available, and therefore they were calculated.

Literature providing kinetic data for cycloalkyl decomposition reactions is very scarce, which makes a comparison of the calculated rate coefficients with previously reported data for these reactions impossible. Instead, the question arises whether the obtained rate coefficients are comparable to the decomposition rates of the smaller units that are present in the tricyclodecyl radicals. *exo*-TCD can be regarded as the joining of a cyclopentane ring and a norbornane bicyclic ring, cf. Scheme 1. Cyclopentyl, derived from cyclopentane, has two

decomposition routes, one C−C β-scission reaction leading to 1-penten-5-yl and one C−H β-scission reaction leading to cyclopentene and H. Norbornane has three different types of carbon atoms, leading to three possible norbornyl radicals, each of which possesses C−C β-scission possibilities. Sirjean et al. provided kinetic data at the CBS-QB3 level of theory for these reactions[63,64] which can be used in comparing the rate coefficients with the tricyclodecyl decomposition reactions.

Rate coefficients for tricyclodecyl reactions with the analogous reactions of cyclopentyl (Figure 1a) and norbornyl radicals (Figure 1b−d) are compared. Rate coefficients of the tricyclodecyl decomposition reactions are smaller than for the analogous reactions of the smaller ring units, up to 1 order of magnitude of difference between β-scission reactions of TCDR4 and cyclopentyl, cf. Figure 1a. In some cases, the joining of the cyclopentane and norbornane rings in tricyclodecyl radicals leads to reactions whose TS structure is not comparable to TSs of the smaller units. Therefore, Figure 1 only compares tricyclodecyl reactions whose TSs are located in one of the two rings.

4.2. Kinetic Model Validation. The generated kinetic model was validated against five data sets of *exo*-TCD pyrolysis experiments. None of the rate coefficients or thermochemical parameters were adjusted by regression of the experimental
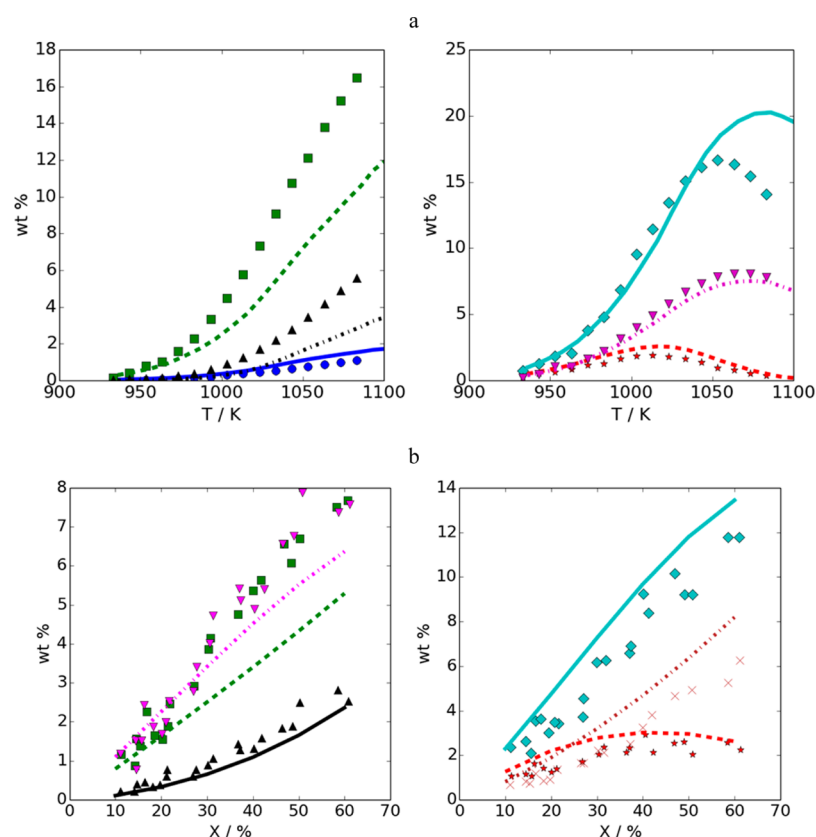
Figure 3. (a) Mass fractions as a function of temperature for the Ghent data.[18] Left: (blue ● and —) dihydrogen, (black ▲ and ·-·-) methane, and (green ■ and ---) ethene. Right: (cyan ◆ and —) 1,3-cyclopentadiene, (magenta ▼ and ·-·-) propene, and (red ★ and ---) cyclopentene. Conditions: 10 mol% JP-10 in N_2 at reactor inlet, $P = 1.7 \times 10^5$ Pa. (b) Mass fractions as a function of *exo*-TCD conversion for the Rao data.[12] Left: (black ▲ and —) methane, (magenta ▼ and ·-·-) propene, and (green ■ and ---) ethene. Right: (red ★ and ---) cyclopentene, (× and ·-·-) benzene, and (cyan ◆ and —) 1,3-cyclopentadiene. Conditions: 100 mol% JP-10 at reactor inlet, $T = 903-968$ K, $P = 1 \times 10^5$ Pa. Symbols are experimental data, and lines are model predictions.

data; i.e., these comparisons are a test of the predictive ability of the model.

Figure 2a shows the *exo*-TCD conversion as a function of the mean reactor temperature for the Ghent data. It can be seen that good agreement is found for all temperatures and both levels of dilution, considering the reported uncertainty on the measurement data.

Figure 2b shows the *exo*-TCD conversion as a function of the equivalent space time for the Rao data. The good agreement between experiments and model predictions indicates that the generated kinetic model performs well for high *exo*-TCD partial pressures. Figure 2c shows the *exo*-TCD conversion as a function of the reactor pressure for the Xing data, the only data set at elevated pressures up to 37×10^5 Pa.[15] While *exo*-TCD conversion is predicted to increase with increasing pressure by the model, the experiments show little influence of pressure on *exo*-TCD conversion at a given temperature. In the experiments of Xing et al.,[15] the reported space time increases by a factor of 50 from the lowest reported pressure relative to the highest pressure and explains why the model predictions for *exo*-TCD conversion at a given temperature increase as a function of pressure. The model predictions are in reasonable agreement at pressures up to 1.8×10^5 Pa and tend to slightly deviate at more elevated pressures. While the Xing experiments are very valuable since they are the only available JP-10 pyrolysis experiments recorded at high pressures, it remains unclear what causes the insensitivity of the experimentally measured JP-10

conversion for the reactor space time and pressure. Figure 2d shows the *exo*-TCD conversion as a function of the residence time for the Nancy data. Good agreement is found between model predictions and experiments, indicating the validity of the model at low conversions under diluted conditions.

Figure 3a shows the mass fractions of the major products as a function of the mean reactor temperature for the Ghent data. Model predictions of propene, CPD, and cyclopentene are in good agreement with the data. The predicted maxima of CPD concentrations are at slightly higher temperatures than experimentally observed. Ethene is consistently underpredicted, which is analyzed in more detail in section 4.3.1 of this work.

Figure 3b shows mass fractions of the major products as a function of the equivalent space time for the Rao data. In this case the agreement between model predictions and experimental data is better than for the Ghent data. The main difference is that in this case model predictions of methane agree with experiments, while methane was slightly underpredicted for the Ghent experiments.

Figure 4 shows the mole fractions of the major products as a function of the mean reactor temperature for the Nancy data. Again, good agreement is found for the majority of the major products and confirms the trends seen in Figure 3.

Mass fractions of the most important formed aromatic species as a function of the mean reactor temperature for the Ghent data are shown in Figure 5a. Besides benzene, the four most significantly formed aromatic species are toluene, styrene,
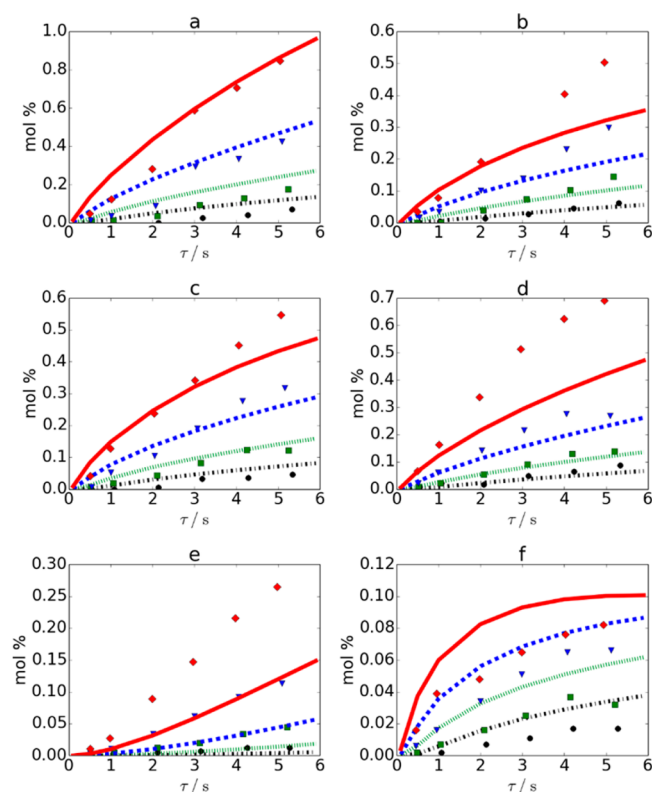
Figure 4. Mole fractions as a function of residence time of (a) dihydrogen, (b) propene, (c) 1,3-cyclopentadiene, (d) ethene, (e) methane, and (f) cyclopentene at four temperatures: ◆, 933; ▼, 913; ■, 893; and ●, 873 K. Lines are model predictions, and symbols are Nancy data.[10] Conditions: 4 mol% *exo*-TCD in He at the reactor inlet, $T = 848-933$ K, $P = 1 \times 10^5$ Pa, conversion = 0.01–25%.

Figure 5. (a) Mass fractions as a function of temperature for the Ghent data.[18] Left: (blue ● and —) benzene, (black ▲ and ⋯) styrene, and (green ■ and ⋯) toluene. Right: (cyan ◆ and —) indene and (magenta ▼ and ⋯) naphthalene. Conditions: 10 mol% JP-10 in N_2 at reactor inlet, $P = 1.7 \times 10^5$ Pa. (b) Mole fractions as a function of residence time for the Nancy data.[10] Left, benzene, and right, toluene, at four temperatures: ◆, 933; ▼, 913; ■, 893; and ●, 873 K. Conditions: 4 mol% *exo*-TCD in He at the reactor inlet, $T = 848-933$ K, $P = 1 \times 10^5$ Pa, conversion = 0.01–25%. Symbols are experimental data, and lines are model predictions.

indene, and naphthalene. Benzene and toluene are slightly underpredicted at temperatures below 1000 K. Indene and naphthalene are overpredicted over the entire temperature range, which could suggest that channels to indene and naphthalene are too much favored over the channels to monoaromatics.

The same trends are observed in Figure 5b that shows mole fractions of benzene and toluene as a function of the mean reactor temperature for the Nancy experiments.

Figure 6 shows the model predictions versus the Nakra and Van Devener data as a function of temperature. Overall, the good agreement between model and experiment indicates that the current model performs well at low pressures and elevated temperatures despite being generated with RMG at significantly different conditions: $T = 1100$ K, $P = 1 \times 10^5$ Pa, 10 mol% *exo*-TCD in N_2. Good agreement is observed for *exo*-TCD conversion. Although both data sets were recorded at similar operating conditions, CPD and ethyne concentrations are underpredicted in the Van Devener data and overpredicted in the Nakra data, while reverse trends are seen for ethene. Less discordant trends are found for benzene. The latter is systematically underpredicted. Benzene model predictions also show a small decrease in benzene mole fractions starting at $T > 1500$ K which was not observed in the experimental data.

The Ghent and Nancy experiments allowed detecting a number of species with very low concentrations. First, the Ghent experiments isolated a number of products containing a five-membered ring, such as methylcyclopentadiene (C_6H_8) and ethenylcyclopentene (C_7H_{10}),[18] cf. Figure 7. Since the
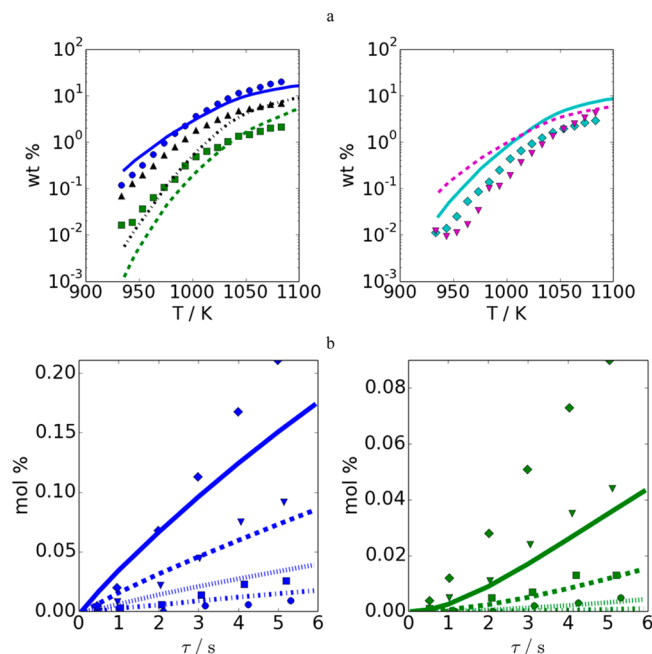
position of the methyl or ethenyl substituent in methylcyclo-pentadiene and ethenylcyclopentene could not be determined, they are compared to model predictions of 1-methyl-1,3-cyclopentadiene and 3-ethenylcyclopentene, respectively. Good agreement between experiments and model predictions is found for the components.

Tricyclo[5.2.1.0^{2,6}]dec-4-ene is another higher molecular weight component that was identified as an important primary decomposition product and which also appears in the current model. As can be seen in Figure 7, the temperature of peak concentration is well predicted, but concentrations are slightly mispredicted.

The overall good agreement between the model predictions and experimentally measured concentrations for a large number of experimental data sets indicates the usefulness of the current model. None of the model parameters were fitted, despite the many uncertainties in kinetics of reactions and thermochemistry of species. This gives an indication of the overall quality of the kinetic model. Finally, remaining discrepancies between model and experiment should be interpreted carefully. Estimated error bars associated with the reported experimental data were rarely reported, making it difficult to judge to which extent the discrepancies are significant. Also, in some of the experiments the boundary conditions are uncertain, and the ideal reactor models employed here are only approximate. Most importantly, despite the best efforts of several researchers including this present work, many of the parameters in this large kinetic model are significantly uncertain, so one would expect significant uncertainties due just to the model. Considering all these factors, the level of agreement between
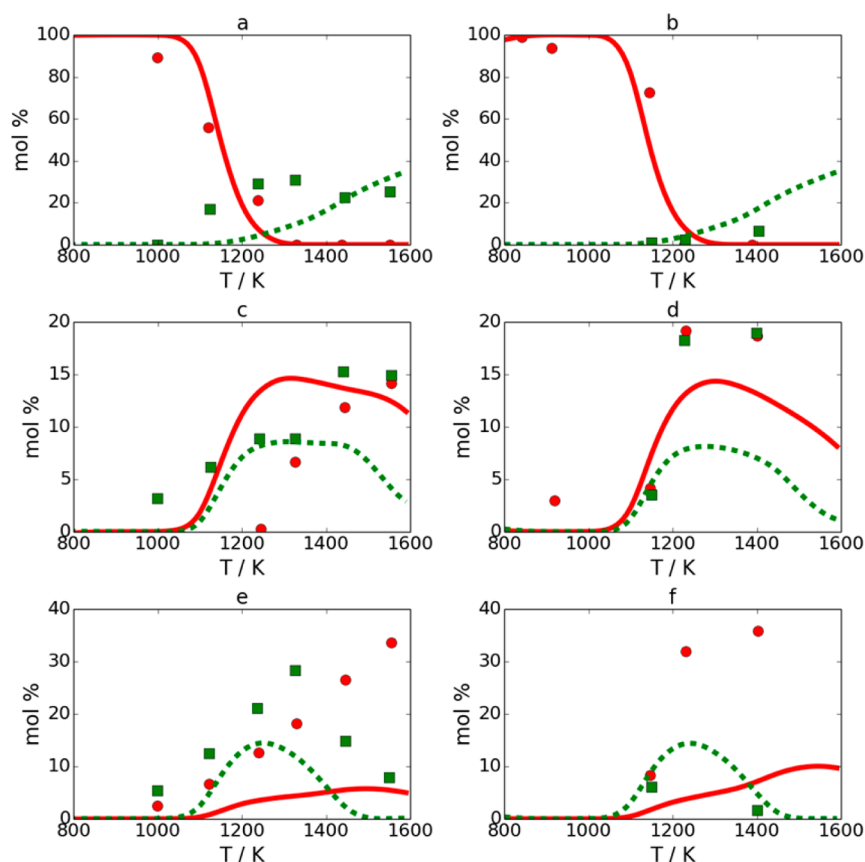
Figure 6. Mole fractions as a function of reactor temperature for model predictions versus Nakra data[13] (left column) and Van Devener data[14] (right column). Experiments (symbols) and model predictions (lines) for (a,b) (red ● and —) *exo*-TCD and (green ■ and ---) ethyne; (c,d) (red ● and —) ethene and (green ■ and ---) propyne; and (e,f) (red ● and —) benzene and (green ■ and ---) 1,3-cyclopentadiene. Conditions for the Nakra[13] and Van Devener[14] data respectively: 2.6/3.9 mol% JP-10 in argon, $P = 300-400/1500-1900$ Pa, conversion = 0–100%.
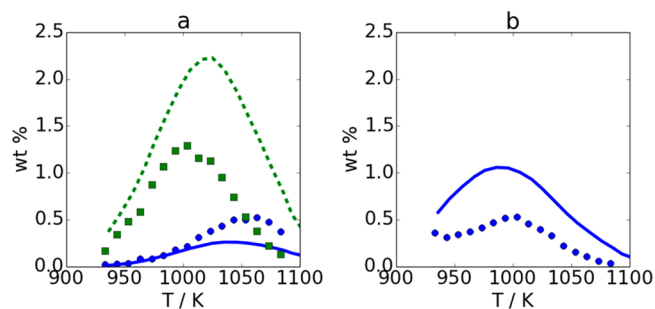

Figure 7. Mass fractions as a function of temperature for the Ghent data[18] for (a) (blue ● and —) 1-methyl-1,3-cyclopentadiene and (green ■ and ---) 3-ethenylcyclopentene, and (b) (● and —) tricyclo[5.2.1.0^{2,6}]dec-4-ene. Conditions: 10 mol% JP-10 in N_2 at reactor inlet, $P = 1.7 \times 10^5$ Pa. Symbols are experimental data, lines are model predictions.

the model predictions and the experiments is very satisfactory, sufficient to justify some more detailed analysis of the reaction paths below.

4.3. Main Reaction Pathways. A schematic representation of the main decomposition pathways of *exo*-TCD predicted by the model for the conditions of the Ghent experiments can be found in Scheme 5. The rates of the important reactions are shown as a percentage relative to the total decomposition rate of *exo*-TCD.

4.3.1. Major Decomposition Pathways of exo-TCD. While the thermal decomposition of *exo*-TCD is initiated by the

scission of a C−C bond yielding BR1, at the conditions corresponding to Scheme 5, 85% of the decomposition rate of *exo*-TCD is accounted for by H-abstraction reactions by H. The main decomposition channels involve TCDR5, TCDR8, and TCDR4 with contributions of 33%, 26%, and 14%, respectively. Decomposition pathways through TCDR7 and TCDR10 are negligible due to the significantly higher bond dissociation energies of the corresponding C−H bonds.[47] The important C_{10} radicals lead to different primary products: TCDR8 leads primarily to cyclopentene and 1,3-cyclopentadiene, with a minor pathway forming benzene and ethyl; TCDR5 leads to 1,4-pentadiene, 1,3-cyclopentadiene, 3-ethenylcyclopentene, and propene; and TCDR4 leads to ethene and 1,3-cyclo-pentadiene via a retro-Diels−Alder reaction of 2-norbornene. A secondary decomposition channel of TCDR4 leads to tricyclo-[5.2.1.0^{2,6}]dec-4-ene and accounts for 45% of the decom-position rate of TCDR4. The channel through TCDR4 is the only significant source of tricyclo[5.2.1.0^{2,6}]dec-4-ene. One of the major uncertainties affecting tricyclo[5.2.1.0^{2,6}]dec-4-ene predictions is the ring strain present in unsaturated species and derived radicals. For example, H-abstraction reactions from tricyclo[5.2.1.0^{2,6}]dec-4-ene result in resonance-stabilized $C_{10}H_{13}$ species containing rings whose ring strain is unknown.

Ethene is initially formed via various primary decomposition routes starting from BR1, TCDR4, TCDR6, and TCDR8. Once propene attains high enough concentrations, the reaction of propene with H atoms resulting in methyl and ethene forms another major ethene formation channel.

Scheme 5. Reaction Pathway Analysis for the Decomposition of *exo*-TCD[a]
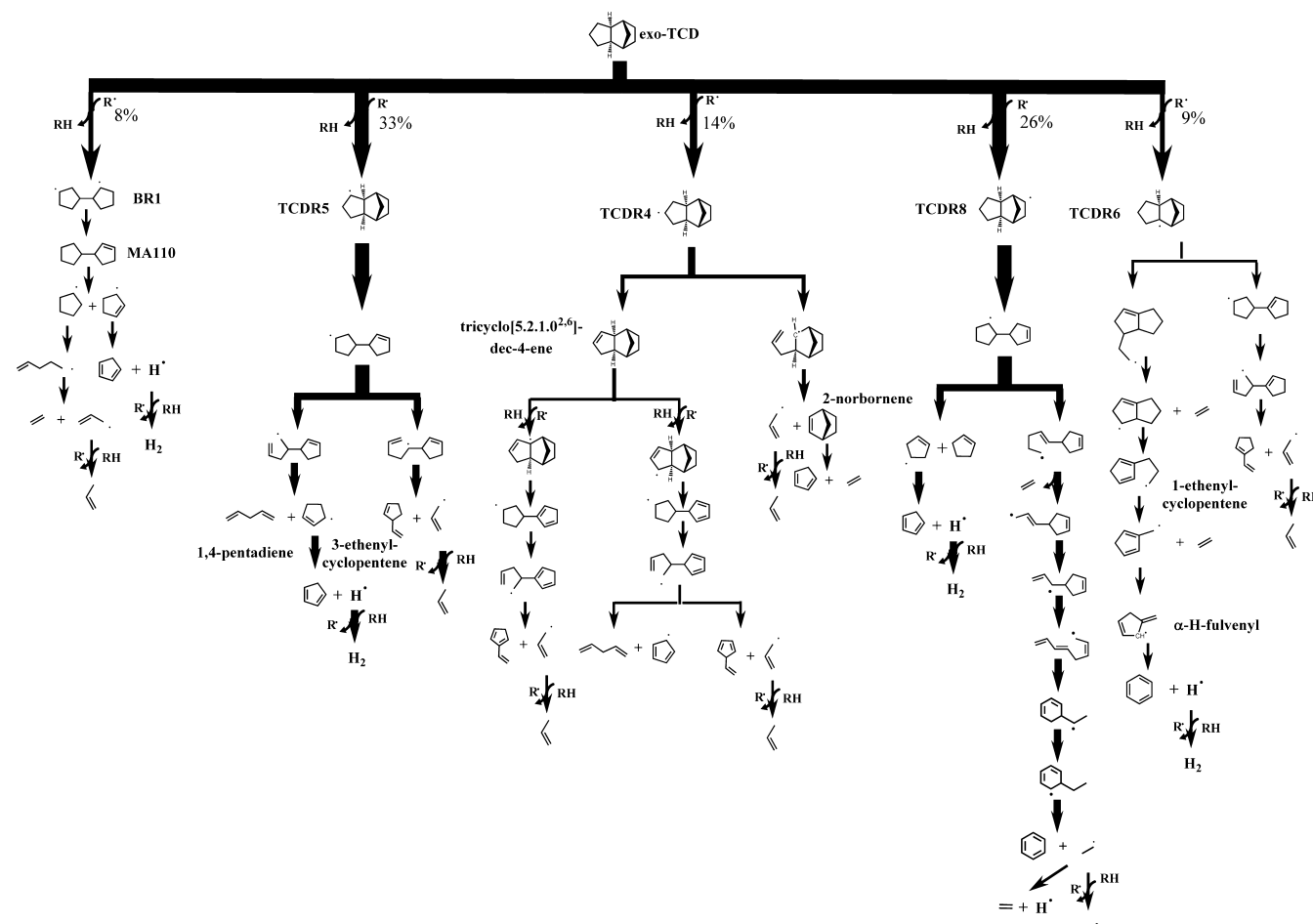
[a]The reported percentages represent the predicted reaction rate relative to the total *exo*-TCD decomposition rate. $T = 1100$ K, $P = 1.7 \times 10^5$ Pa, conversion$_{exo\text{-TCD}}$ = 19%, 10 mol% *exo*-TCD in N_2 corresponding to conditions of the Ghent data set. Only major *exo*-TCD decomposition pathways are shown.
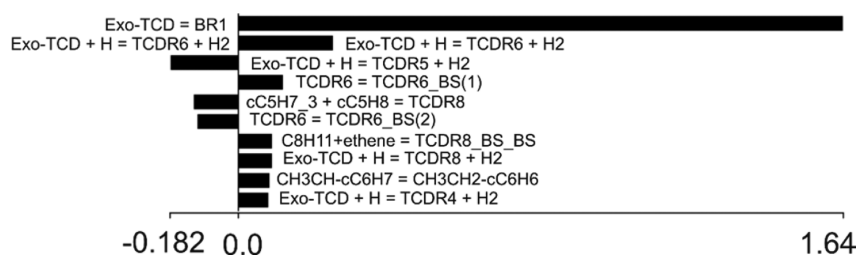

Figure 8. Normalized sensitivity coefficients for ethene at $T = 1100$ K, $P = 1.5 \times 10^5$ Pa, corresponding to an *exo*-TCD conversion = 16%. "BS" indicates that the species represents is formed through a β-scission reaction of the reactant.

The observation that ethene concentrations are underestimated over most of the data sets at lower temperatures raises questions on the source of the discrepancy. One potential source is the lack of pathways leading toward ethene, e.g., because of the exclusion of reaction families such as intramolecular 1,4- and 1,5-H-abstraction reactions. It is possible that the tricyclodecyl or other derived radicals that do not lead to ethene may isomerize to other C_{10} radicals that do eventually decompose into ethene. Second the accuracy of rate coefficients can be questioned. Sensitivity analysis was used to quantitatively assess the importance of rate coefficients. Normalized sensitivity coefficients S_{ij} for pre-exponential factors

A_j of reaction j on the mole fraction of species X_i were calculated using Chemkin-Pro.

Figure 8 shows that ethene has a very large positive sensitivity coefficient for the primary decomposition channel through BR1. This channel is the major *exo*-TCD initiation pathway through which a pool of H atoms and allyl radicals is established. These radicals are the most important moieties that subsequently consume *exo*-TCD. Not surprisingly, ethene is also sensitive to reactions that influence the branching of tricyclodecyl radicals, such as the consumption of *exo*-TCD by H yielding TCDR6. These reactions directly influence the fraction of *exo*-TCD molecules that lead to ethene.
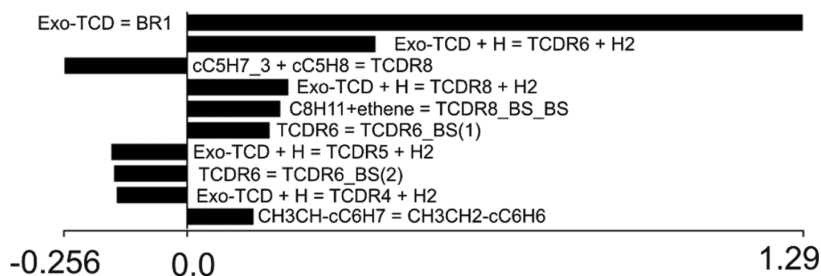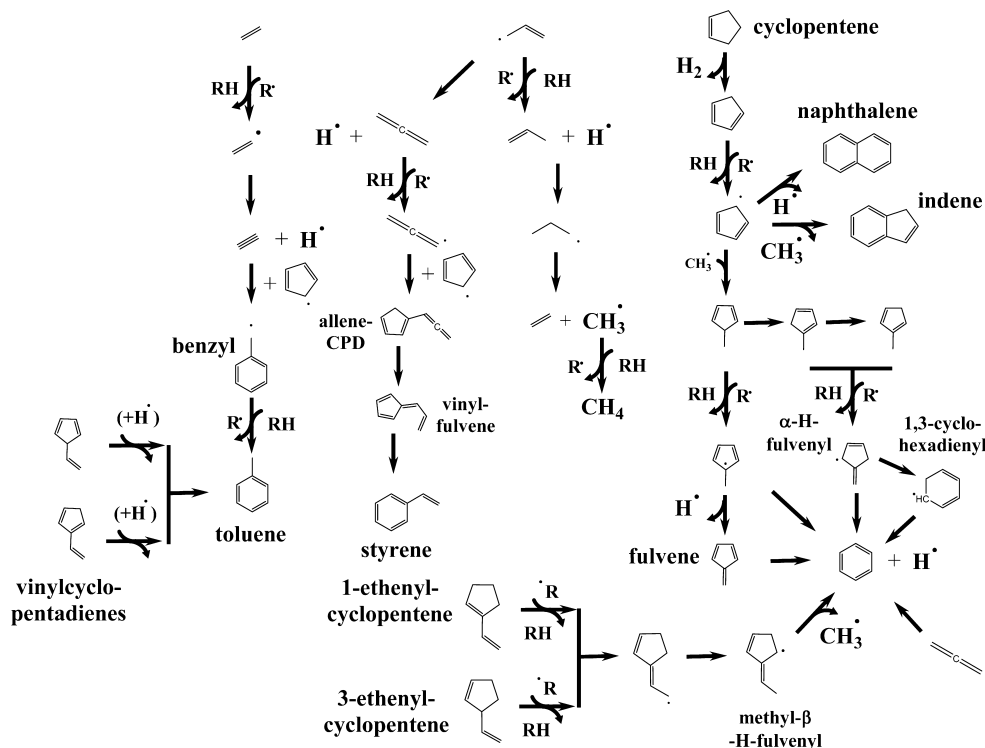
Scheme 6. Pathways of Secondary Conversion of Primary Products Relevant at T = 1100 K, P = 1.7 × 10^5 Pa

Figure 9. Normalized sensitivity coefficients for benzene at T = 1100 K, P = 1.7 × 10^5 Pa, corresponding to an *exo*-TCD conversion = 36%. "BS" indicates that the species represents is formed through a β-scission reaction of the reactant.

Since 1,3-cyclopentadiene is slightly overpredicted, it is possible that the deviating ethene concentration can be attributed to small errors on the rate coefficients for the H-abstractions by H from *exo*-TCD. Moreover, since reverse rate coefficients are calculated through thermodynamic consistency, uncertain estimates of thermochemistry may play a role, too.

Furthermore, the overprediction of tricyclo[5.2.1.0^{2,6}]dec-4-ene is correlated with the underprediction of ethene, as less TCDR4 is decomposing through the competing channel that produces ethene. A major factor of uncertainty is the ring strain in the unsaturated tricyclo[5.2.1.0^{2,6}]decene rings. At the conditions in Scheme 5, benzene is primarily formed via two channels of primary decomposition of *exo*-TCD, which account for 90% of the total rate of production of benzene;46% of benzene is formed through the primary decomposition channel starting from TCDR6 through α-H-fulvenyl, cf. Scheme 5. The second important benzene formation pathway starts from TCDR8 and proceeds via a series of rearrangements of C$_8$H$_{11}$, eventually resulting in benzene and ethyl.

4.3.2. Secondary Chemistry and Aromatics Formation. Many studies of JP-10 pyrolysis indicated the presence of significant quantities of aromatic components, with benzene,

toluene, styrene, indene, and naphthalene as the most prominent species.[10,12] The current model suggests that major *exo*-TCD decomposition pathways lead to hydrogen, ethene, propene, CPD, cyclopentene, and ethenylcyclopentenes. These primary products represent the hydrocarbon pool from which secondary products such as aromatics are formed. CPD and the derived CPDyl radical play a central role in the formation of aromatic species.[65] A schematic overview of important secondary pathways is depicted in Scheme 6.

At higher *exo*-TCD conversion, H-abstraction reactions convert CPD into CPDyl, with allyl and H the most important abstracting radicals. Routes from CPD/CPDyl to indene and naphthalene form the two most important ways of consumption of CPD, both accounting for 30% of the total decomposition rate of CPDyl. Naphthalene formation kinetics were based on the reaction proposed by Lindstedt et al.[66] It involves a two-step sequence in which CPDyl radicals recombine to the stabilized C$_5$H$_5$−C$_5$H$_4$ moiety, which rearranges to naphthalene. Kinetics of the indene formation route by addition of CPDyl to CPD originate from Cavallotti et al.,[31] reported at P = 1.1 × 10^5 Pa.

Secondary conversion of cyclopentene leads to 1,3-cyclopentadiene, with the direct dehydrogenation pathway accounting for ca. 80% of the total cyclopentene decomposition rate. The conversion of propene produces methyl radical and is the second major source for methyl radicals. The latter recombine with CPDyl yielding 5-methylcyclopentadiene. This C_6H_8 molecule can rearrange into the other methylcyclopentadiene isomers or can undergo H-abstraction resulting in methyl-1,3-cyclopentadien-5-yl and isomeric H-fulvenyl radicals. The latter rearrange via various exit channels to fulvene, 1,3-cyclohexadienyl and eventually benzene. The kinetics and thermochemistry for these reactions and species were taken from Sharma and Green.[30]

Another important aspect of the kinetic model at high *exo*-TCD conversion is the secondary conversion of ethenylcyclopentenes. The latter produce fulvene and represents an important pathway to α-H-fulvenyl, cf. Scheme 6. Next to the primary decomposition channels from TCDR6 and TCDR8, the hydrogen-assisted fulvene isomerization and the decomposition of 5-methyl-1,3-cyclopentadien-5-yl[30] become importance sources of benzene, too. A sensitivity analysis of benzene predictions at 1100 K is shown in Figure 9 and illustrates again the importance of the unimolecular ring-opening reaction of *exo*-TCD yielding BR1, initiating the chemistry.

The majority of the reactions shown in Figure 9 were based on estimations by analogy from RMG's databases. More accurate rate coefficients for these reactions based on *ab initio* techniques may therefore be valuable.

5. CONCLUSIONS

A detailed kinetic model was developed to simulate JP-10 pyrolysis using the RMG software. New elements of this model compared to previously developed JP-10 models are the inclusion of more accurate kinetics for initial *exo*-TCD decomposition chemistry, improved fused ring thermochemistry, and the incorporation of many secondary conversion routes to aromatics.

The good agreement between model predictions and five independent sets of experimental data was surprising, given the uncertainty in many parameters in the model and without adjustment of any of the model parameters to experimental data. Significant differences exist between the newly calculated CBS-QB3 rate coefficients of the tricyclodecyl radical decomposition reactions and literature values for the rate coefficients of the smaller analogous units of norbornane and cyclopentyl, illustrating that the use of rate coefficients from analogous reactions to model JP-10 decomposition reactions could lead to inaccurate results. It not only indicated the usefulness and validity of the kinetic model over a wide range of conditions but also confirmed the value of RMG as a tool for the kinetic modeling of complex decomposition chemistry of PAHs.

Analysis of the kinetic model showed the importance of four important H-abstraction reactions from *exo*-TCD besides the unimolecular initiation route leading to 3-cyclopentylcyclopentene and indicated that each of these routes leads to primary products such as hydrogen, ethene, propene, 1,3-cyclopentadiene, cyclopentenes, ethenylcyclopentenes, and benzene. Next to the primary decomposition reactions, a large part of the model involves detailed kinetics for the secondary conversion of primary products toward aromatics such as toluene and styrene. These components are formed through the secondary conversion of unsaturated five-membered rings such as

ethenylcyclopentenes and 1,3-cyclopentadiene-derived moieties. Polyaromatic hydrocarbons such as indene and naphthalene are formed primarily by molecular growth reactions of cyclopentadienyl/cyclopentadiene moieties rather than direct dehydrogenation routes from *exo*-TCD, as also shown by Djokic et al.[65]

■ ASSOCIATED CONTENT

ⓢ Supporting Information

Section S1, modified Arrhenius parameter fit; section S2, mechanism development considerations; section S3, *ab initio* reaction barriers at 0 K; and section S4, kinetic model in Chemkin format. This material is available free of charge via the Internet at http://pubs.acs.org.

■ AUTHOR INFORMATION

Corresponding Author

*E-mail: mariefrancoise.reyniers@ugent.be. Phone: +32 (0)9 264 5677.

Notes

The authors declare no competing financial interest.

■ ACKNOWLEDGMENTS

■ REFERENCES

(1) Chung, H. S.; Chen, C. S. H.; Kremer, R. A.; Boulton, J. R.; Burdette, G. W. Recent developments in high-energy density liquid hydrocarbon fuels. *Energy Fuels* **1999**, *13* (3), 641−649.

(2) Meylemans, H. A.; Baldwin, L. C.; Harvey, B. G. Low-Temperature Properties of Renewable High-Density Fuel Blends. *Energy Fuels* **2013**, *27* (2), 883−888.

(3) Outcalt, S. L.; Laesecke, A. Measurements of Density and Speed of Sound of JP-10 and a Comparison to Rocket Propellants and Jet Fuels. *Energy Fuels* **2011**, *25* (3), 1132−1139.

(4) Billaud, F.; Chaverot, P.; Freund, E. Cracking of Decalin and Tetralin in the Presence of Mixtures of N-decane and Steam at about 810-degrees-C. *J. Anal. Appl. Pyrol.* **1987**, *11*, 39−53.

(5) Cooper, M.; Shepherd, J. E. *Thermal and Catalytic Cracking of JP-10 for Pulse Detonation Engine Applications*; Graduate Aeronautical Laboratories, California Institute of Technology: Pasadena, CA, 2002.

(6) Heneghan, S. P.; Harrison, W. E. JP-8+100: The Development of High Thermal Stability Jet Fuel. 6th International Conference on Stability and Handling of Liquid Fuels, Vancouver, Canada, 1997.

(7) Huang, H.; Sobel, D. R.; Spadaccini, L. J., Endothermic Heat-Sink of Jet Fuels for Scramjet Cooling. 38th AIAA/ASME/SAE/ASEE Joint Propulsion Conference and Exhibit, Indianapolis, IN, 2002.

(8) Colket, M. B.; Spadaccini, L. J. Scramjet fuels autoignition study. *J. Propul. Power* **2001**, *17* (2), 315−323.

(9) Edwards, T. Advancements in Gas Turbine Fuels From 1943 to 2005. *J. Eng. Gas Turbines Power* **2007**, *129* (1), 13−20.

(10) Herbinet, O.; Sirjean, B.; Bounaceur, R.; Fournet, R.; Battin-Leclerc, F.; Scacchi, G.; Marquaire, P. M. Primary mechanism of the thermal decomposition of tricyclodecane. *J. Phys. Chem. A* **2006**, *110* (39), 11298−11314.

(11) Davidson, D. F.; Horning, D. C.; Oehlschlaeger, M. A.; Hanson, R. K., The Decomposition Products of JP-10. 37th Joint Propulsion Conference, Salt Lake City, UT2001; AIAA 01-3707.

(12) Rao, P. N.; Kunzru, D. Thermal cracking of JP-10: Kinetics and product distribution. *J. Anal. Appl. Pyrol.* **2006**, *76* (1–2), 154–160.

(13) Nakra, S.; Green, R. J.; Anderson, S. L. Thermal decomposition of JP-10 studied by micro-flowtube pyrolysis-mass spectrometry. *Combust. Flame* **2006**, *144* (4), 662–674.

(14) Van Devener, B.; Anderson, S. L. Breakdown and combustion of JP-10 fuel catalyzed by nanoparticulate CeO2 and Fe2O3. *Energy Fuels* **2006**, *20* (5), 1886–1894.

(15) Xing, Y.; Fang, W. J.; Xie, W. J.; Guo, Y. S.; Lin, R. S. Thermal Cracking of JP-10 under Pressure. *Ind. Eng. Chem. Res.* **2008**, *47* (24), 10034–10040.

(16) Wohlwend, K.; Maurice, L. Q.; Edwards, T.; Striebich, R. C.; Vangsness, M.; Hill, A. S. Thermal stability of energetic hydrocarbon fuels for use in combined cycle engines. *J. Propul. Power* **2001**, *17* (6), 1258–1262.

(17) Seiser, R.; Niemann, U.; Seshadri, K. Experimental study of combustion of n-decane and JP-10 in non-premixed flows. *Proc. Combust. Inst.* **2011**, *33*, 1045–1052.

(18) Vandewiele, N. M.; Magoon, G. R.; Van Geem, K. M.; Reyniers, M.-F.; Green, W. H.; Marin, G. B. Experimental and Modeling Study on the Thermal Decomposition of Jet Propellant-10. *Energy Fuels* **2014**, *28* (8), 4976–4985.

(19) Li, S. C.; Varatharajan, B.; Williams, F. A. Chemistry of JP-10 ignition. *Am. Inst. Aeronautics Astronautics J.* **2001**, *39* (12), 2351–2356.

(20) Magoon, G. R.; Aguilera-Iparraguirre, J.; Green, W. H.; Lutz, J. J.; Piecuch, P.; Wong, H. W.; Oluwole, O. O. Detailed chemical kinetic modeling of JP-10 (exo-tetrahydrodicyclopentadiene) high-temperature oxidation: Exploring the role of biradical species in initial decomposition steps. *Int. J. Chem. Kinet.* **2012**, *44* (3), 179–193.

(21) Green, W. H.; Allen, J. W.; Ashcraft, R. W.; Beran, G. J.; Class, C. A.; Gao, C.; Goldsmith, C. F.; Harper, M. R.; Jalan, A.; Magoon, G. R.; Matheu, D. M.; Merchant, S. S.; Mo, J. D.; Petway, S.; Raman, S.; Sharma, S.; Song, J.; Van Geem, K. M.; Wen, J.; West, R. H.; Wong, A.; Wong, H. S.; Yelvington, P. E.; Yu, J. RMG—Reaction Mechanism Generator v4.0; 2013.

(22) Song, J.; Raman, S.; Yu, J.; Wijaya, C. D.; Stephanopoulos, G.; Green, W. H. Development of automatic chemical reaction mechanism generation software using object-oriented technology. *Abstracts of Papers*, 226th National Meeting of the American Chemical Society, New York, NY, Sept 7–11,2003; pp U530–U531.

(23) Song, J. Building Robust Chemical Reaction Mechanisms: Next Generation of Automatic Model Construction Software. Ph.D thesis, MIT, 2004.

(24) Susnow, R. G.; Dean, A. M.; Green, W. H.; Peczak, P.; Broadbelt, L. J. Rate-based construction of kinetic models for complex systems. *J. Phys. Chem. A* **1997**, *101* (20), 3731–3740.

(25) Harper, M. R.; Van Geem, K. M.; Pyl, S. P.; Marin, G. B.; Green, W. H. Comprehensive reaction mechanism for n-butanol pyrolysis and combustion. *Combust. Flame* **2011**, *158* (1), 16–41.

(26) Sabbe, M. K.; Van Geem, K. M.; Reyniers, M.-F.; Marin, G. B. First Principle-Based Simulation of Ethane Steam Cracking. *AIChE J.* **2011**, *57* (2), 482–496.

(27) Van Geem, K. M.; Reyniers, M. F.; Marin, G. B.; Song, J.; Matheu, D. M.; Green, W. H. Automatic Reaction Network Generation using RMG for Steam Cracking of n-Hexane. *AIChE J.* **2006**, *52* (2), 718–730.

(28) Hughes, K. J.; Turanyi, T.; Clague, A. R.; Pilling, M. J. Development and testing of a comprehensive chemical mechanism for the oxidation of methane. *Int. J. Chem. Kinet.* **2001**, *33* (9), 513–538.

(29) Sharma, S.; Harper, M. R.; Green, W. H. Modeling of 1,3-hexadiene, 2,4-hexadiene and 1,4-hexadiene-doped methane flames: Flame modeling, benzene and styrene formation. *Combust. Flame* **2010**, *157* (7), 1331–1345.

(30) Sharma, S.; Green, W. H. Computed Rate Coefficients and Product Yields for c-C5H5 + CH3 → Products. *J. Phys. Chem. A* **2009**, *113* (31), 8871–8882.

(31) Cavallotti, C.; Polino, D.; Frassoldati, A.; Ranzi, E. Analysis of Some Reaction Pathways Active during Cyclopentadiene Pyrolysis. *J. Phys. Chem. A* **2012**, *116* (13), 3313–3324.

(32) Zhang, L.; Cai, J.; Zhang, T.; Qi, F. Kinetic modeling study of toluene pyrolysis at low pressure. *Combust. Flame* **2010**, *157* (9), 1686–1697.

(33) Benson, S. W. *Thermochemical Kinetics*; John Wiley & Sons: New York, 1976.

(34) Magoon, G. R.; Green, W. H. Design and implementation of a next-generation software interface for on-the-fly quantum and force field calculations in automated reaction mechanism generation. *Comput. Chem. Eng.* **2013**, *52*, 35–45.

(35) Magoon, G.; Green, W. H.; Oluwole, O. O.; Wong, H. W.; Albo, S. E.; Lewis, D. K. Updating Our Understanding of JP-10 Decomposition Chemistry: A Detailed JP-10 Combustion Mechanism Constructed Using RMG—an Automatic Reaction Mechanism Generator. 46th AIAA/ASME/SAE/ASEE Joint Propulsion Conference & Exhibit, Nashville, TN, 2010.

(36) Poling, B. E.; Prausnitz, J. M.; O'Connel, J. P. *The properties of gases and liquids*; McGraw-Hill: New York, 2001.

(37) Wiberg, K. B. The Concept of Strain in Organic-Chemistry. *Angew. Chem., Int. Ed. Engl.* **1986**, *25* (4), 312–322.

(38) Gasteiger, J.; Dammer, O. Automatic Estimation of Ring Strain Energies. *Tetrahedron* **1978**, *34* (19), 2939–2945.

(39) Verevkin, S. P.; Emel'yanenko, V. N.; Pimerzin, A. A.; Vishnevskaya, E. E. Thermodynamic Analysis of Strain in Heteroatom Derivatives of Indene. *J. Phys. Chem. A* **2011**, *115* (44), 12271–12279.

(40) Verevkin, S. P.; Emel'yanenko, V. N.; Pimerzin, A. A.; Vishnevskaya, E. E. Thermodynamic Analysis of Strain in the Five-Membered Oxygen and Nitrogen Heterocyclic Compounds. *J. Phys. Chem. A* **2011**, *115* (10), 1992–2004.

(41) Landrum, G. RDKit: Open-source cheminformatics, http://rdkit.sourceforge.net, 2006.

(42) Lay, T. H.; Bozzelli, J. W.; Dean, A. M.; Ritter, E. R. Hydrogen-atom bond increments for calculation of thermodynamic properties of hydrocarbon radical species. *J. Phys. Chem.* **1995**, *99* (39), 14514–14527.

(43) Nunes, P. M.; Estacio, S. G.; Lopes, G. T.; Costa Cabral, B. J.; Borges dos Santos, R. M.; Martinho Simoes, J. A. C—H Bond Dissociation Enthalpies in Norbornane. An Experimental and Computational Study. *Org. Lett.* **2008**, *10* (8), 1613–1616.

(44) McMillen, D. F.; Golden, D. M. Hydrocarbon Bond-Dissociation Energies. *Annu. Rev. Phys. Chem.* **1982**, *33*, 493–532.

(45) Tian, Z. X.; Fattahi, A.; Lis, L.; Kass, S. R. Cycloalkane and cycloalkene C-H bond dissociation energies. *J. Am. Chem. Soc.* **2006**, *128* (51), 17087–17092.

(46) Feng, Y.; Liu, L.; Wang, J. T.; Zhao, S. W.; Guo, Q. X. Homolytic C-H and N-H bond dissociation energies of strained organic compounds. *J. Org. Chem.* **2004**, *69* (9), 3129–3138.

(47) Hudzik, J. M.; Asatryan, R.; Bozzelli, J. W. Thermochemical Properties of exo-Tricyclo 5.2.1.0(2,6) decane (JP-10 Jet Fuel) and Derived Tricyclodecyl Radicals. *J. Phys. Chem. A* **2010**, *114* (35), 9545–9553.

(48) Castano, O.; Notario, R.; Abboud, J. L. M.; Gomperts, R.; Palmeiro, R.; Frutos, L. M. Organic thermochemistry at high ab initio levels. 2. Meeting the challenge: Standard heats of formation of gaseous norbornane, 2-norbornene, 2,5-norbornadiene, cubane, and adamantane at the G2 level. *J. Org. Chem.* **1999**, *64* (25), 9015–9018.

(49) Walsh, R.; Wells, J. M. Enthalpy of Formation of Bicyclo[2.2.1]-hepta-2,5-diene - Thermodynamic Functions of Bicyclo[2.2.1]heptane and Bicyclo[2.2.1]hepta-2,5-diene. *J. Chem. Thermodyn.* **1975**, *7* (2), 149–154.

(50) An, X. W.; Zhu, H. P.; Hu, R. H. Heats of Combustion and Formation of Norbornane. *Thermochim. Acta* **1987**, *121*, 473–477.

(51) Celani, P.; Werner, H. J. Multireference perturbation theory for large restricted and selected active space reference wave functions. *J. Chem. Phys.* **2000**, *112* (13), 5546–5557.

(52) Werner, H. J. Third-order multireference perturbation theory—The CASPT3 method. *Mol. Phys.* **1996**, *89* (2), 645–661.

(53) Werner, H.-J.; Knowles, P. J.; Knizia, G.; Manby, F. R.; Schutz, M.; Celani, P.; Korona, T.; Lindh, R.; Mitrushenkov, A.; Rauhut, G.; Shamasundar, K. R.; Adler, T. B.; Amos, R. D.; Bernhardsson, A.; Berning, A.; Cooper, D. L.; Deegan, M. J. O.; Dobbyn, A. J.; Eckert, F.; Goll, E.; Hampel, C.; Hesselmann, A.; Hetzer, G.; Hrenar, T.; Jansen, G.; Koppl, C.; Liu, Y.; Lloyd, A. W.; Mata, R. A.; May, A. J.; McNicholas, S. J.; Meyer, W.; Mura, M. E.; Nicklass, A.; O'Neill, D. P.; Palmieri, P.; Peng, D.; Pfluger, K.; Pitzer, R.; Reiher, M.; Shiozaki, T.; Stoll, H.; Stone, A. J.; Tarroni, R.; Thorsteinsson, T.; Wang, M. *MOLPRO*, version 2012.1, a package of ab initio programs.

(54) Sirjean, B.; Glaude, P. A.; Ruiz-Lopez, M. F.; Fournet, R. Detailed kinetic study of the ring opening of cycloalkanes by CBS-QB3 calculations. *J. Phys. Chem. A* **2006**, *110* (46), 12693−12704.

(55) Sirjean, B.; Fournet, R.; Glaude, P.-A.; Ruiz-López, M. F. Extension of the composite CBS-QB3 method to singlet diradical calculations. *Chem. Phys. Lett.* **2007**, *435* (1−3), 152−156.

(56) Eckart, C. The penetration of a potential barrier by electrons. *Phys. Rev.* **1930**, *35* (11), 1303−1309.

(57) Sharma, S.; Harper, M. R.; Green, W. H. *CANTHERM*, 2010.

(58) *CHEMKIN-PRO*, 150101; Reaction Design: San Diego, 2009.

(59) Van Geem, K. M.; Pyl, S. P.; Marin, G. B.; Harper, M. R.; Green, W. H. Accurate High-Temperature Reaction Networks for Alternative Fuels: Butanol Isomers. *Ind. Eng. Chem. Res.* **2010**, *49* (21), 10399−10420.

(60) Bruno, T. J.; Huber, M. L.; Laesecke, A.; Lemmon, E. W.; Perkins, R. A. Thermochemical and Thermophysical Properties of JP-10, NISTIR 6640; National Institute of Standards and Technology, June 2006.

(61) O'Neal, H. E.; Benson, S. W. Biradical Mechanism in Small Ring Compound Reactions. *J. Phys. Chem.* **1968**, *72* (6), 1866−1887.

(62) Dean, A. M.; Bozzelli, J. W. Combustion chemistry of nitrogen. In *Gas-phase combustion chemistry*; Gardiner, W., Ed.; Springer: Berlin, 2000; pp 125−341.

(63) Sirjean, B.; Herbinet, O.; Glaude, P.-A.; Ruiz-Lopez, M.; Fournet, R. Theoretical Study of the Thermal Decomposition of a Jet Fuel Surrogate. WSS/CI Spring 2008 Meeting, University of Southern California, March 17−18, 2007.

(64) Sirjean, B.; Glaude, P. A.; Ruiz-Lopez, M. F.; Fournet, R. Theoretical Kinetic Study of Thermal Unimolecular Decomposition of Cyclic Alkyl Radicals. *J. Phys. Chem. A* **2008**, *112* (46), 11598−11610.

(65) Djokic, M.; Van Geem, K.; Cavallotti, C.; Frassoldati, A.; Ranzi, E.; Marin, G. An experimental and kinetic modeling study of cyclopentadiene pyrolysis: First growth of polycyclic aromatic hydrocarbons. *Combust. Flame* **2014**, *161* (11), 2739−2751.

(66) Lindstedt, P.; Maurice, L.; Meyer, M. Thermodynamic and kinetic issues in the formation and oxidation of aromatic species. *Faraday Discuss.* **2001**, *119*, 409−432.